

Surface Tension Effects on Surface Instabilities of Dielectric Elastomers

Saman Seifi^a, Qiming Wang^b, Harold S. Park^c

^aDepartment of Mechanical Engineering, Boston University, Boston, MA 02215

^bDepartment of Civil and Environmental Engineering, University of Southern California, Los Angeles, CA 90089

^cDepartment of Mechanical Engineering, Boston University, Boston, MA 02215

Abstract

Dielectric elastomers have recently been proposed for various biologically-relevant applications, in which they may operate in fluidic environments where surface tension effects may have a significant effect on their stability and reliability. Here, we present a theoretical analysis coupled with computational modeling for a generalized electromechanical analysis of surface stability in dielectric elastomers accounting for surface tension effects. For mechanically deformed elastomers, significant increases in critical strain and instability wavelength are observed for small elastocapillary numbers. When the elastomers are deformed electrostatically, both surface tension and the amount of pre-compression are found to substantially increase the critical electric field while decreasing the instability wavelength.

Keywords: Wrinkling Instability, Elastocapillary, Perturbation Analysis

1. Introduction

Because soft materials like gels and elastomers often operate under states of compression, there have been significant efforts to examine their mechanical stability under such loading (Biot, 1963; Gent and Cho, 1999; Biot and Romain, 1965; Tanaka et al., 1987; Gent, 2005; Hong et al., 2009). Recently, efforts have focused on examining the stability of surfaces due to the formation of instabilities such as wrinkles and creases under compression (Cao and Hutchinson, 2012; Li et al., 2012; Jin et al., 2014; Cai et al., 2012; Hong and Gao, 2013; Weiss et al., 2013). The studies of wrinkling instabilities have typically been analytical in nature, based on linear perturbation analysis, which enables predictions of critical strains and instability wavelengths in these soft structures. These studies have also been insightfully combined with experiments (Cai et al., 2010, 2012; Jin et al., 2015), and also numerical (finite element) analyses (Cao and Hutchinson, 2012; Jin and Suo, 2015; Jin et al., 2015; Wang and Zhao, 2014, 2016).

More recently, linear perturbation analyses have been applied to an interesting class of soft, active materials - dielectric elastomers (DEs). These materials have drawn significant interest due to the large deformations they can undergo resulting from applied electrostatic loading (Carpi et al., 2010; Brochu and Pei, 2010; Biddiss and Chau, 2008; Mirfakhrai et al., 2007). Furthermore, DEs often form surface instabilities like creasing, wrinkling and cratering, which have been studied via experiment, theory and computation (Suo, 2010; Plante and Dubowsky, 2006; Zhou et al., 2008; Wang et al., 2012; Shivapooja et al., 2013;

Wang et al., 2011; Wang and Zhao, 2013; Park et al., 2012, 2013), and also using analytic techniques based on stability analyses (Zhao and Suo, 2007, 2009) and the nonlinear field theory of Suo et al. (2008).

While DEs have drawn significant interest in recent years, many promising technological innovations, such as generating electromechanical motion during magnetic resonance imaging (Carpi et al., 2008), operating soft, underwater robots (Rus and Tolley, 2015; Kim et al., 2013), manipulating microfluidic flow (Holmes et al., 2013), focusing a tunable lens (Carpi et al., 2011), the preparation of bioinspired surfaces (Shivapooja et al., 2013), underwater grippers (Laschi et al., 2012) and soft body locomotion (Marchese et al., 2014), involve operation of the DE in fluidic environments, where elastocapillary effects due to surface tension can become prominent (Roman and Bico, 2010; Liu and Feng, 2012). While prior works have examined either the effects of surface tension alone on surface instabilities in elastomers (Chen et al., 2012) and hydrogels (Kang and Huang, 2010), or the coupled effects of surface tension and electric fields on surface instabilities in constrained DE films (Wang and Zhao, 2013; Seifi and Park, 2016; Wang et al., 2016), a general stability analysis of compressed DE films subject to both surface tension and electric fields has not been performed.

The objective of this work is to present a theoretical analysis coupled with computational modeling for surface tension effects on surface instabilities in DEs, with particular emphasis on surface instability wavelengths, and critical strains or electric fields needed to induce the surface instabilities. We consider first the case of surface tension effects on a mechanically compressed DE film, then move on to consider the general case of electrostatic loading on

URL: samansei@bu.edu (Saman Seifi), qimingw@usc.edu (Qiming Wang), parkhs@bu.edu (Harold S. Park)

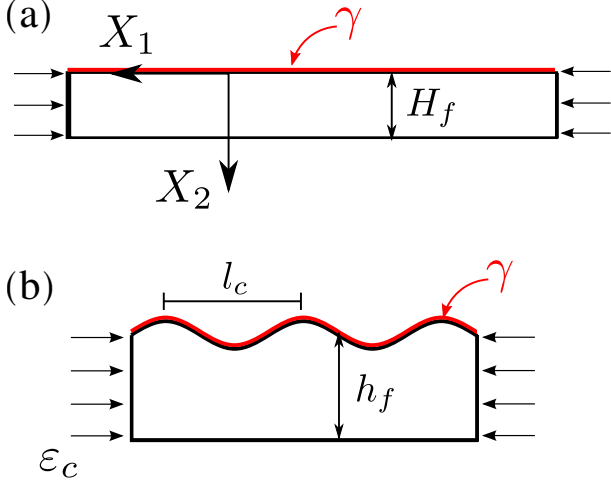


Figure 1: A perfectly flat film subject to compression and surface tension γ . (a) Undeformed configuration; (b) the formation of wrinkles with wavelength l_c .

a mechanically compressed DE film.

2. Governing Equations and Incremental Forms

We first present, for a DE film subject to surface tension and under compressive loading, the governing equations and their incremental forms. We assume that the surface of the film is subject to Young-Laplace boundary conditions in order to account for elastocapillary effects on the surface (Saksono and Peric, 2006). We initially neglect the effects of applied electrostatic loading (i.e. voltages or electric fields), which will be accounted for in the subsequent section. The perturbation analysis we utilize is based on those performed by Cai et al. (2010); Kang and Huang (2010); Jin et al. (2014, 2015)

2.1. Dielectric Elastomer Subject to Surface Tension

We first consider a DE film under compression, that is also subject to surface tension effects on its top surface, as illustrated in Figure (1). The deformation of the body is described by the field $\mathbf{x}(\mathbf{X})$. The deformation gradient is:

$$F_{iK} = \frac{\partial x_i(\mathbf{X})}{\partial X_K} \quad (1)$$

The DE is modeled as an incompressible neo-Hookean material with the free energy function:

$$W(\mathbf{F}) = \frac{\mu}{2} F_{iK} F_{iK} - \pi (\det \mathbf{F} - 1) \quad (2)$$

The nominal stress s_{iK} can be derived as:

$$s_{iK} = \frac{\partial W(\mathbf{F})}{\partial F_{iK}} = \frac{\mu}{J} F_{iK} - \pi H_{iK} \quad (3)$$

where $\mathbf{H} = \mathbf{F}^{-T}$, μ is the shear modulus, and $\pi = \pi(\mathbf{X})$ is the Lagrange multiplier to enforce the constraint of incompressibility: $J = \det \mathbf{F} = 1$. The nominal stress satisfies

the equilibrium equation:

$$\frac{\partial s_{iK}}{\partial X_K} = 0 \quad (4)$$

On the surface of the body the film is subjected to the Young-Laplace boundary condition (Saksono and Peric, 2006) with surface tension γ :

$$s_{iK} N_K dA = 2\gamma \kappa n_i da \quad (5)$$

where \mathbf{N} is the unit normal vector to the surface of the body in the undeformed state, \mathbf{n} is the unit normal vector in the current state, and κ is the mean curvature of the surface.

We now add a perturbation into the state of finite deformation with position $x_i^0(\mathbf{X})$, deformation gradient $F_{iK}^0(\mathbf{X})$ and nominal stress $s_{iK}^0(\mathbf{X})$. If the deformation in the z -direction is constrained, only 2D deformation is considered. The deformation gradient of this state is

$$\mathbf{F}^0 = \begin{bmatrix} \lambda & 0 \\ 0 & 1/\lambda \end{bmatrix} \quad (6)$$

Therefore the corresponding position is $\mathbf{x}^0 = \mathbf{F}^0 \mathbf{X}$. Now by adding a small displacement perturbation of $\dot{\mathbf{x}}$, we write the perturbed state as $\mathbf{x} = \mathbf{x}^0(\mathbf{X}) + \dot{\mathbf{x}}(\mathbf{X})$. Both state $\mathbf{x}^0(\mathbf{X})$ and the perturbed state $\mathbf{x}^0(\mathbf{X}) + \dot{\mathbf{x}}(\mathbf{X})$ satisfy the same governing equations in (1) and (4). The incremental form of the deformation gradient reduces to

$$\dot{F}_{iK} = \frac{\partial \dot{x}_i(\mathbf{X})}{\partial X_K} \quad (7)$$

and the equilibrium equation to

$$\frac{\partial \dot{s}_{iK}}{\partial X_K} = 0 \quad (8)$$

where the incremental nominal stress can be obtained using Taylor's expansion at \mathbf{F}^0 of the stress in (3):

$$\dot{s}_{iK} = \mu \dot{F}_{iK} - \dot{\pi} H_{iK}^0 + \pi^0 H_{iL}^0 H_{jK}^0 \dot{F}_{jL} \quad (9)$$

Inserting (9) into (8) we can obtain the following equation:

$$(\mu \delta_{ij} \delta_{KL} + \pi^0 H_{iL}^0 H_{jK}^0) \frac{\partial^2 \dot{x}_j(\mathbf{X})}{\partial X_K \partial X_L} - H_{iK}^0 \frac{\partial \dot{\pi}}{\partial X_K} = 0 \quad (10)$$

The perturbation of the incompressibility condition becomes

$$H_{iK}^0 \dot{F}_{iK} = 0 \quad (11)$$

where the perturbation of the boundary-condition is:

$$\dot{s}_{iK} N_K = 2\gamma \dot{\kappa} H_{iK}^0 N_K + 2\gamma \kappa \dot{H}_{iK}^0 N_K \quad (12)$$

Finally, the boundary condition on the top the film (12) reduces to

$$\dot{s}_{iK} N_K = 2\gamma \dot{\kappa} H_{iK}^0 N_K \quad (13)$$

where the term involving κ in (12) drops out as $\kappa = 0$. At the bottom of the film, we have the boundary conditions:

$$\dot{s}_{12} = 0 \quad \text{and} \quad \dot{x}_2 = 0 \quad (14)$$

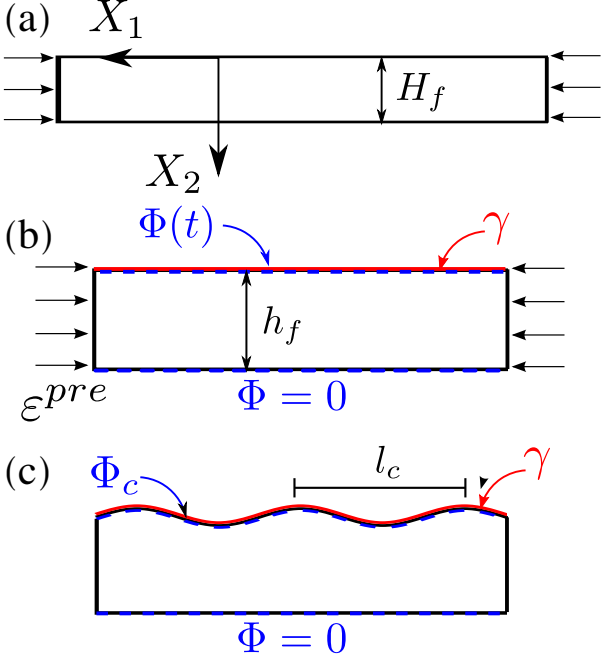


Figure 2: A perfectly flat film subject to compression, electric field and surface tension γ . (a) Undeformed configuration; (b) Compressed to a given strain ε^{pre} , after which voltage $\Phi(t)$ is applied to the top surface while $\Phi = 0$ on the bottom surface; (c) The formation of wrinkles with critical wavelength l_c at critical electric potential Φ_c .

2.2. Dielectric Elastomer with Surface Tension and Electric Field Effects

We now consider the general problem of interest, that of a DE film that is subject to compressive loading, while accounting for both surface tension and electrostatic loading via electric fields. This is illustrated in Figure (2). In this case, the reference state is a pre-compressed plane strain film, subject to the deformation gradient

$$\mathbf{F}^{pre} = \begin{bmatrix} \lambda^{pre} & 0 \\ 0 & 1/\lambda^{pre} \end{bmatrix} \quad (15)$$

For this film, the net deformation gradient between the current state and the undeformed state is $F_{iK}F_{Km}^{pre}$, and the free energy of equation in (2) becomes

$$W(\mathbf{F}) = \frac{\mu}{2} F_{iK} F_{Km}^{pre} F_{iL} F_{Lm}^{pre} - \pi(\det \mathbf{F} - 1) \quad (16)$$

and therefore the nominal stress of (3) becomes

$$s_{iK} = \frac{\mu}{J} F_{Km}^{pre} F_{Lm}^{pre} F_{iL} - \pi H_{iK}. \quad (17)$$

At this state (Figure 2-b), an electric potential Φ is applied on top of the film along with the surface tension γ . When the elastomer is at the flat state, the electric field in the elastomer film is homogeneous, with the electric field vector as

$$\mathbf{E} = \begin{bmatrix} 0 \\ E_2 \end{bmatrix} \quad (18)$$

where $E_2 = \Phi/h_f$ is the applied electric field where $h_f = H_f/\lambda^{pre}$ is the height of the pre-compressed film.

The electric field \mathbf{E} generates an extra stress \mathbf{s}^e inside the film. The nominal electric stress can be calculated as $\mathbf{s}^e = J\sigma^e\mathbf{H}^0$ where $\sigma^e = \epsilon\mathbf{E} \otimes \mathbf{E} - \frac{\epsilon}{2}|\mathbf{E}|^2\mathbf{I}$. Also here $\mathbf{H}^0 = (\mathbf{F}^0)^{-T}$ where \mathbf{F}^0 is the deformation gradient that describes the post-compressed motion. Therefore we can obtain the nominal electric stress as

$$\mathbf{s}^e = J \begin{bmatrix} -\frac{1}{2}\epsilon E_2^2 & 0 \\ 0 & \frac{1}{2}\epsilon E_2^2 \end{bmatrix} \mathbf{H}^0. \quad (19)$$

The equilibrium equation becomes

$$\frac{\partial(s_{iK} + s_{iK}^e)}{\partial X_K} = 0 \quad (20)$$

With relation (19), and the fact that the film remains flat before the onset of surface wrinkling, we have the approximation $\mathbf{F}^0 \approx \mathbf{I}$ and therefore $(\mathbf{F}^0)^{-T} = \mathbf{H}^0 \approx \mathbf{I}$, we can obtain $\frac{\partial s_{iK}^e}{\partial X_K} \approx 0$. Thus the stress equilibrium reduces to:

$$\frac{\partial s_{iK}}{\partial X_K} = 0 \quad (21)$$

Now similar to the previous case, we perturb the post-compressed state of deformation, of displacement x_i^0 and deformation gradient \mathbf{F}^0 . The incremental state of stress becomes:

$$\dot{s}_{iK} = \mu F_{Km}^{pre} F_{Lm}^{pre} \dot{F}_{jL} + \pi^0 H_{iL}^0 H_{jK}^0 \dot{F}_{jL} - H_{iK}^0 \dot{\pi} \quad (22)$$

and the equilibrium equation becomes:

$$\frac{\partial \dot{s}_{iK}}{\partial X_K} = 0 \quad (23)$$

where it can be rewritten as:

$$(\mu F_{Km}^{pre} F_{Lm}^{pre} \delta_{ij} + \pi^0 H_{iL}^0 H_{jK}^0) \frac{\partial^2 x_j}{\partial X_K \partial X_L} - H_{iL}^0 \frac{\partial \dot{\pi}}{\partial X_K} = 0 \quad (24)$$

After rearrangement of electric stress the boundary condition on top of the film is:

$$\dot{s}_{iK} N_K = 2\gamma \dot{\kappa} n_i - \dot{s}_{iK}^e N_K \quad (25)$$

where according to (19) we have $\dot{s}_{iK}^e = \dot{\sigma}_{ij}^e$ as a consequence of the fact that $\mathbf{H}^0 \approx \mathbf{I}$. By assuming the fact that the DE film undergoes a sinusoidal undulation with small amplitude δ at the onset of wrinkling, the electric field then is $(E_2)_\delta = \Phi/(h_f + \delta)$, and therefore the linear approximation of the electrical stress using Taylor's series becomes:

$$\dot{\sigma}^e = \begin{bmatrix} \epsilon E_2^2 \left(\frac{\delta}{h_f} \right) & 0 \\ 0 & -\epsilon E_2^2 \left(\frac{\delta}{h_f} \right) \end{bmatrix} \quad (26)$$

And finally the boundary conditions at the bottom of the film is fixed:

$$\dot{x}_1(X_1, H_f) = \dot{x}_2(X_1, H_f) = 0 \quad (27)$$

3. Linear Perturbation Analysis for Wrinkles

3.1. Compression with elastocapillary effect

To determine the onset of wrinkling, we require the existence of non-trivial solutions to the eigenvalue problem corresponding to the incremental boundary value problems derived in the previous section. Separated solution exists in the incremental boundary value problem with the perturbation in the following form:

$$\begin{aligned}\dot{x}_1(X_1, X_2) &= f_1(X_2) \sin(KX_1) \\ \dot{x}_2(X_1, X_2) &= f_2(X_2) \cos(KX_1) \\ \dot{\pi}(X_1, X_2) &= f_3(X_2) \cos(KX_1)\end{aligned}\quad (28)$$

Substituting these equations into (10) we obtain

$$f_2'''' - K^2(\lambda^{-4} + 1)f_2'' + K^4\lambda^{-4}f = 0 \quad (29)$$

The derivatives of f_2 are with respect to X_2 and $K = 2\pi/L$ is the wave number. The wavelength in the reference state L relates to wavelength in current l state by $L = l/\lambda$. The ODE in (29), accompanied with the boundary conditions in (13) and (14), leads to an eigenvalue problem, of which the non-trivial solutions correspond to the wrinkling state. The corresponding algebraic equation of the following form then can be obtained

$$\mathbf{A} \begin{bmatrix} C_1 \\ C_2 \\ C_3 \\ C_4 \end{bmatrix} = 0 \quad (30)$$

The existence of a non-trivial solution to the perturbed boundary value problem requires

$$\det \mathbf{A} = 0 \quad (31)$$

where matrix $\det \mathbf{A}$ can be written as a function of $\det \mathbf{A} = f(\lambda, KH_f, \gamma/(\mu H_f))$. The explicit expression of this matrix is given as follows:

$$\begin{aligned}A_{11} &= -\frac{\gamma KH_f}{\lambda \mu} - H_f K \left(\lambda^2 + \frac{1}{\lambda^2} \right) \\ A_{12} &= -\frac{\gamma KH_f}{\lambda \mu} + H_f K \left(\lambda^2 + \frac{1}{\lambda^2} \right) \\ A_{13} &= -\frac{\gamma H_f K^2}{\mu \lambda} - 2KH_f \\ A_{14} &= -\frac{\gamma H_f K^2}{\mu \lambda} + 2KH_f\end{aligned}\quad (32)$$

$$\begin{aligned}A_{21} &= A_{22} = \frac{2KH_f}{\lambda^2} \\ A_{23} &= A_{24} = \lambda^2 KH_f + \frac{KH_f}{\lambda^2}\end{aligned}\quad (33)$$

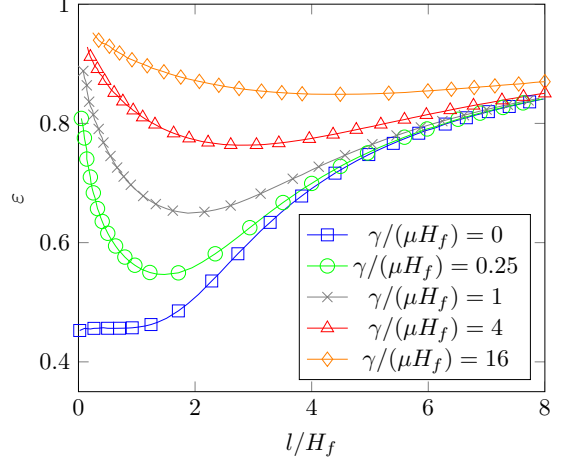


Figure 3: Strain vs. wavelength for a range of elastocapillary numbers

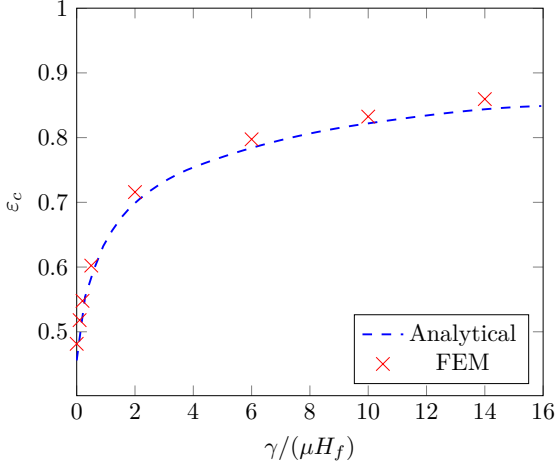
$$\begin{aligned}A_{31} &= \frac{2KH_f e^{-KH_f \lambda^{-2}}}{\lambda^2} \\ A_{32} &= \frac{2KH_f e^{KH_f \lambda^{-2}}}{\lambda^2} \\ A_{33} &= \lambda^2 KH_f e^{-KH_f} + \frac{KH_f e^{-KH_f}}{\lambda^2} \\ A_{34} &= \lambda^2 KH_f e^{KH_f} + \frac{KH_f e^{KH_f}}{\lambda^2}\end{aligned}\quad (34)$$

$$\begin{aligned}A_{41} &= e^{-KH_f \lambda^{-2}}, \quad A_{42} = e^{KH_f \lambda^{-2}} \\ A_{43} &= e^{-KH_f}, \quad A_{44} = e^{KH_f}\end{aligned}\quad (35)$$

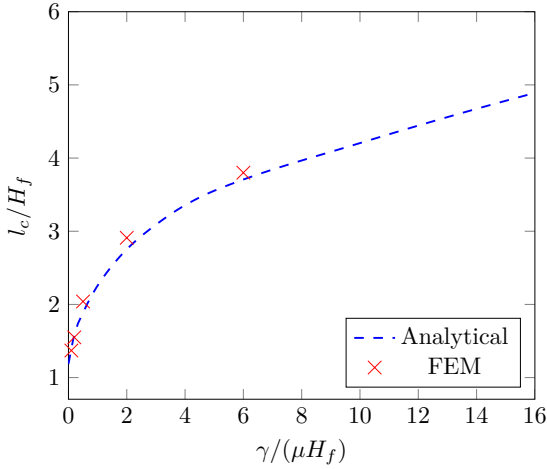
By solving the eigenvalue problem in (31), we obtain the relation between stretch λ , and therefore the compressive strain $\varepsilon = 1 - \lambda$ with the wavelength l (Figure 3). For each curve, the minimal critical strain $\varepsilon_c = 1 - \lambda_c$ reaches a minimum for wrinkles of certain wavelength l_c . The relation of these critical values with elastocapillary number $\gamma/(\mu H_f)$ is plotted in Figure 4.

When surface tension is neglected ($\gamma = 0$), we recover Biot's value of wrinkling at $\varepsilon_w \approx 0.46$ as shown in Figure 3 (Biot, 1963). When surface tension is present ($\gamma > 0$), the strain ε first decreases and then increases as the normalized wavelength l/H_f increases (Figure 3). The key effect of surface tension is that it inhibits bifurcation, as both the critical strain ε_c and corresponding normalized wavelength l_c/H_f increase with increasing $\gamma/(\mu H_f)$ (Figure 4). These results are consistent with previous studies on surface tension effects on surface instabilities (Chen et al., 2012), and are expected since a smaller wavelength l/H_f implies a larger energy penalty in terms of surface energy (Shenoy and Sharma, 2001).

In addition, we find that for large elastocapillary numbers, the critical strain approaches a limiting value of $\varepsilon_c \approx 0.85$. The largest change in critical strain occurs for small elastocapillary numbers, i.e. $0 \leq \gamma/(\mu H_f) \leq 2$, where the change in ε_c is more than 34% from $\varepsilon_c = 0.46$



(a)



(b)

Figure 4: (a): Critical strain ε_c vs. elasto-capillary number $\gamma/(\mu H_f)$; (b): Critical wavelength l_c/H_f vs. elasto-capillary number $\gamma/(\mu H_f)$

for $\gamma/(\mu H_f) = 0$ to $\varepsilon_c \approx 0.7$ for $\gamma/(\mu H_f) = 2$, while for $\gamma/(\mu H_f) > 2$ the increase in ε_c is less than 18% (Figure 4a).

The solutions to the critical wavelength are different from the critical strain in that there is no limit to the wavelength. As with the critical strain in Figure 4a, a rapid increase in normalized wavelength is observed for small elastocapillary numbers. For $\gamma/(\mu H_f) > 4$, where the change in critical strain is not significant, the normalized wavelength continues increasing in a linear fashion.

We also verified the theoretical model by performing dynamic, nonlinear finite element (FE) calculations using the methodology for electro-elastocapillary phenomena in DEs previously developed by Seifi and Park (2016), while neglecting the electrostatic effects, thus considering a purely mechanical problem. All numerical simulations using open source simulation code Tahoe (2015) using standard 4-node, bilinear quadrilateral finite elements within a

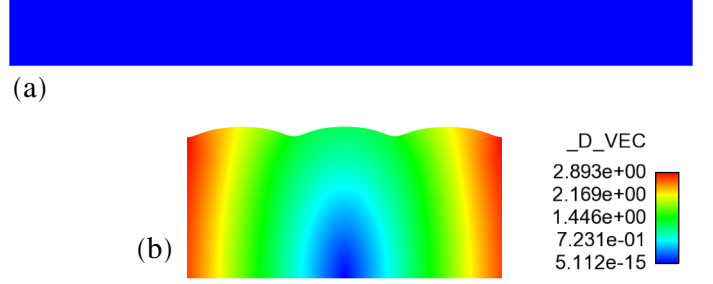


Figure 5: Results for FE simulation of a mechanical compression-induced instability of an 40×4 elastomer film. (a) Undeformed film (b) Onset of wrinkling instability on the top surface at the critical strain $\varepsilon_c = 0.547$ and elastocapillary number $\gamma/(\mu H_f) = 0.2$. $_D_VEC$ is the displacement magnitude.

two-dimensional, plane strain approximation. Simulations were performed on a elastomer film with length $L_f = 40$ and height of $H_f = 4$ with a mesh size of $d = 1/16$.

In the FE simulations, we measured the critical strain ε_c as soon as the wrinkling pattern on surface appears, see for example (Figure 5). For the comparisons to the critical strain in Figure 4(a), the FE results match the theoretical model very closely. For the normalized wavelength l_c/H_f in Figure 4(b), the FE results match also closely match the theoretical model. However, we were not able to obtain the wavelength of the wrinkles for $\gamma/(\mu H_f) > 2$ where the film is more than %70 compressed due to the computational expense needed in modeling very long films.

3.2. Compressed film subject to surface tension and electric field

To account for electromechanical coupling on the compression-induced instability, we substitute equations in (28) into (24) giving the following differential equation:

$$f_2'''' - K^2 ((\lambda^{pre})^4 + 1) f_2'' + K^4 (\lambda^{pre})^4 f_2 = 0. \quad (36)$$

This equation along with the boundary conditions in (25) and (27) gives the second algebraic equation:

$$\mathbf{B} \begin{bmatrix} C_1 \\ C_2 \\ C_3 \\ C_4 \end{bmatrix} = 0 \quad (37)$$

The existence of a non-trivial solution requires:

$$\det \mathbf{B} = 0 \quad (38)$$

where the matrix $\det \mathbf{B}$ can be written as function of dimensionless parameters $\det \mathbf{B} = g(KH_f, \tilde{E} \sqrt{\epsilon/\mu}, \gamma/(\mu H_f))$ and the stretch λ^{pre} is a prescribed constant and where $\tilde{E} = \Phi/H_f$ is the nominal

electric field. The explicit expression of the matrix \mathbf{B} is:

$$\begin{aligned}
B_{11} &= -\frac{(\lambda^{pre})^2 \Phi^2 \epsilon}{\mu H_f^2} - \frac{\gamma H_f K^2}{\mu(\lambda^{pre})} - 2KH_f \\
B_{12} &= -\frac{(\lambda^{pre})^2 \Phi^2 \epsilon}{\mu H_f^2} - \frac{\gamma H_f K^2}{\mu(\lambda^{pre})} + 2KH_f \\
B_{13} &= -\frac{(\lambda^{pre})^2 \Phi^2 \epsilon}{\mu H_f^2} - \frac{\gamma H_f K^2}{\mu(\lambda^{pre})} \\
&\quad - KH_f \left((\lambda^{pre})^2 + \frac{1}{(\lambda^{pre})^2} \right) \\
B_{14} &= -\frac{(\lambda^{pre})^2 \Phi^2 \epsilon}{\mu H_f^2} - \frac{\gamma H_f K^2}{\mu(\lambda^{pre})} \\
&\quad + KH_f \left((\lambda^{pre})^2 + \frac{1}{(\lambda^{pre})^2} \right) \\
B_{21} &= B_{22} = -(\lambda^{pre})^2 KH_f - \frac{KH_f}{(\lambda^{pre})^2} \\
B_{23} &= B_{34} = -\frac{2KH_f}{(\lambda^{pre})^2} \\
B_{31} &= (\lambda^{pre})^2 KH_f \left(-e^{-H_f K(\lambda^{pre})} \right) \\
B_{32} &= (\lambda^{pre})^2 KH_f \left(e^{H_f K(\lambda^{pre})} \right) \\
B_{33} &= KH_f \left(-e^{-\frac{KH_f}{(\lambda^{pre})^2}} \right), \quad B_{34} = KH_f \left(e^{\frac{KH_f}{(\lambda^{pre})^2}} \right) \\
B_{41} &= e^{-KH_f(\lambda^{pre})}, \quad B_{42} = e^{KH_f(\lambda^{pre})} \\
B_{43} &= e^{-\frac{KH_f}{(\lambda^{pre})^2}}, \quad B_{44} = e^{\frac{KH_f}{(\lambda^{pre})^2}}
\end{aligned} \tag{39}$$

$$\begin{aligned}
B_{21} &= B_{22} = -(\lambda^{pre})^2 KH_f - \frac{KH_f}{(\lambda^{pre})^2} \\
B_{23} &= B_{34} = -\frac{2KH_f}{(\lambda^{pre})^2}
\end{aligned} \tag{40}$$

$$\begin{aligned}
B_{31} &= (\lambda^{pre})^2 KH_f \left(-e^{-H_f K(\lambda^{pre})} \right) \\
B_{32} &= (\lambda^{pre})^2 KH_f \left(e^{H_f K(\lambda^{pre})} \right)
\end{aligned} \tag{41}$$

$$\begin{aligned}
B_{33} &= KH_f \left(-e^{-\frac{KH_f}{(\lambda^{pre})^2}} \right), \quad B_{34} = KH_f \left(e^{\frac{KH_f}{(\lambda^{pre})^2}} \right) \\
B_{41} &= e^{-KH_f(\lambda^{pre})}, \quad B_{42} = e^{KH_f(\lambda^{pre})} \\
B_{43} &= e^{-\frac{KH_f}{(\lambda^{pre})^2}}, \quad B_{44} = e^{\frac{KH_f}{(\lambda^{pre})^2}}
\end{aligned} \tag{42}$$

The solution to the eigenvalue problem in (38) gives the relation between the nominal electric field and the wavelength at a given stretch λ^{pre} for various elastocapillary numbers. For instance, Figure 6 shows the calculated nominal electric-field $\tilde{E} \sqrt{\epsilon/\mu}$ for inducing the wrinkling instabilities in DEs for a uniaxial compression of $\epsilon^{pre} = 0.2$. The normalized nominal electric-field first decreases and then increases as the wavelength increases. The lowest electric-field in each curve gives the critical nominal electric-field $\tilde{E}_c \sqrt{\epsilon/\mu}$ for wrinkling instability.

We have recovered the analytic result in Wang and Zhao (2013) for wrinkling instability of a film without pre-compression $\epsilon^{pre} = 0$, as shown in Figure 7. The results in Figure 7 also demonstrate that pre-compressing the DE film leads to a significant increase in the electric field that is needed to induce the surface wrinkling instability, i.e. a near doubling of the voltage is needed as the initial compressive strain increases from 0 to 40%. Pre-stretch has been widely observed to decrease the nominal electric field required for pull-in instability (Zhao and Suo, 2007), thus compression induces the opposite effect, that of increasing the nominal electric field \tilde{E} required for electromechanical instability.

Increasing the surface tension, and thus the elastocapillary number has a similar effect, in that the critical nominal electric field needed to induce surface wrinkling increases substantially for a given pre-compression as the

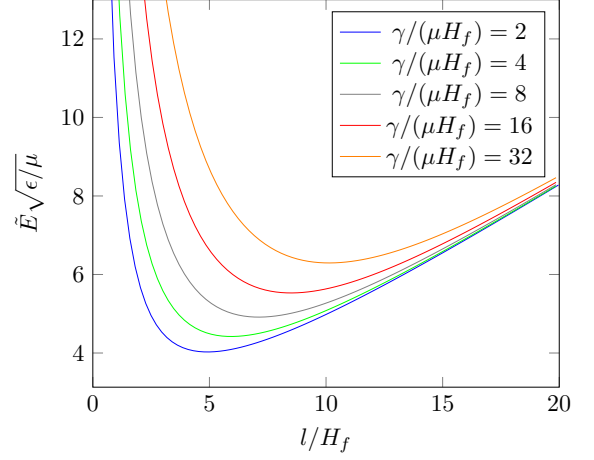


Figure 6: Analytic solution for $\lambda^{pre} = 0.8$ (or $\epsilon^{pre} = 0.2$) shows normalized nominal electric field vs. normalized wavelength for various elastocapillary numbers $\gamma/(\mu H_f)$

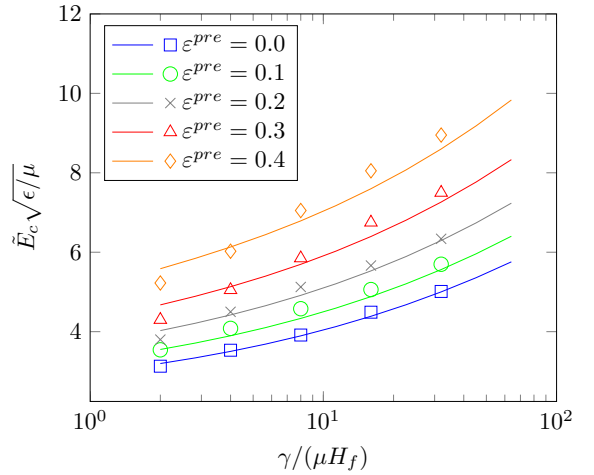


Figure 7: Critical electric field vs. elastocapillary number. The solid lines are the analytical results and the corresponding markers are the finite element solutions.

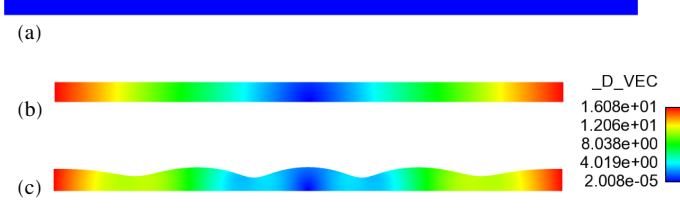


Figure 8: FE simulation for electrically induced instability of a 160×4 DE film. (a) Undeformed film (b) Compressed film (in this case $\varepsilon^{pre} = 0.2$) (c) Wrinkled structure due to applied electric field and surface tension (here $\gamma/(\mu H_f) = 8$).

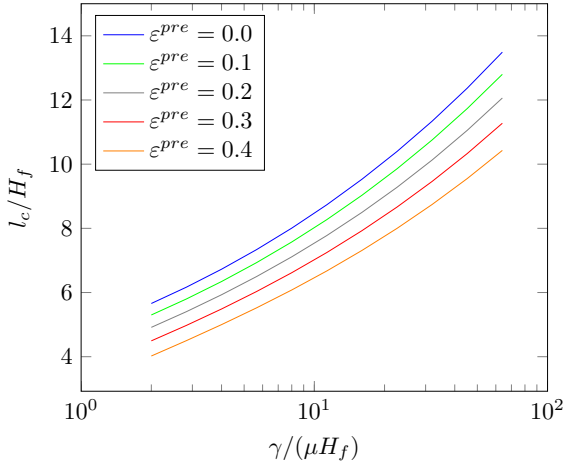


Figure 9: Analytic solution of critical wavelength vs. elasto-capillary number.

elastocapillary number increases. Again, a near-doubling of the critical electric field is needed as the elastocapillary number increases from 1 to 100.

These results were verified using the nonlinear FE method of Seifi and Park (2016). To study the surface instability of a pre-compressed film subjected to electric field, we first statically compress a film with length of $L_f = 160$ and height $H_f = 4$ with mesh size $d = 1/16$ to various strains of $\varepsilon^{pre} = 0.1, 0.2, 0.3$ and 0.4 , all of which are smaller than Biot's wrinkling strain $\varepsilon_w = 0.46$. Once the film is compressed, an electric potential on top of the film is applied (Figure 2-b) in conjunction with surface tension γ . The electric potential Φ was then increased linearly with time until the surface wrinkling instability occurs, where an illustration of the resulting surface wrinkling instability that is observed is shown in Figure 8. The normalized critical nominal electric field $\tilde{E}_c \sqrt{\epsilon/\mu}$ is then measured as soon as the wrinkles appears on the surface. In Figure 7, this critical electric field is plotted using symbols as a function of elastocapillary number $\gamma/(\mu H_f)$. The FE results are in a good agreement with our perturbation analysis.

Finally, Figure 9 shows that for a given elastocapillary number, the wrinkling wavelength decreases with increas-

ing DE film compressive strain. This trend is opposite from Figure 4, where the wavelength increases with increasing elastocapillary number. This is because the pre-compressive strain ε^{pre} reduces the surface area. This reduction in surface area also reduces the surface energy, which results in a decrease in the critical wavelength.

4. Conclusions

In conclusion, we have presented a theoretical model augmented with computational analysis to examine the surface instabilities of dielectric elastomers accounting for surface tension effects. Surface tension is found to significantly impact the nature of the surface instabilities in the DEs, both through increasing the electric fields required to induce the instability, as well as in increasing the wavelength of the resulting instability. We note that in the purely mechanical compression of soft materials, creases always occur before wrinkles regardless of the surface tension value (Chen et al., 2012). However, in electromechanically coupled soft materials like DEs, wrinkles occur before creases when the elastocapillary number is larger than one (Wang and Zhao, 2013). Indeed, here we have focused on the analysis for elastocapillary numbers larger than one, as illustrated in Figs. 8 and 9.

5. Acknowledgements

HSP and SS acknowledge funding from the ARO, grant W911NF-14-1-0022.

References

- Biddiss, E., Chau, T., 2008. Dielectric elastomers as actuators for upper limb prosthetics: challenges and opportunities. *Medical Engineering and Physics* 30, 403–418.
- Biot, M., 1963. Surface instability of rubber in compression. *Applied Scientific Research, Section A* 12, 168–182.
- Biot, M.A., Romain, J.E., 1965. Mechanics of incremental deformations. *Physics Today* 18, 68.
- Brochu, P., Pei, Q., 2010. Advances in dielectric elastomers for actuators and artificial muscles. *Macromolecular Rapid Communications* 31, 10–36.
- Cai, S., Bertoldi, K., Wang, H., Suo, Z., 2010. Osmotic collapse of a void in an elastomer: breathing, buckling and creasing. *Soft Matter* 6, 5770–5777.
- Cai, S., Chen, D., Suo, Z., Hayward, R.C., 2012. Creasing instability of elastomer films. *Soft Matter* 8, 1301–1304.
- Cao, Y., Hutchinson, J.W., 2012. Wrinkling phenomena in neo-hookean film/substrate bilayers. *Journal of applied mechanics* 79, 031019.
- Carpi, F., Bauer, S., Rossi, D.D., 2010. Stretching dielectric elastomer performance. *Science* 330, 1759–1761.
- Carpi, F., Frediani, G., Turco, S., De Rossi, D., 2011. Bioinspired tunable lens with muscle-like electroactive elastomers. *Advanced Functional Materials* 21, 4152–4158.
- Carpi, F., Khanicheh, A., Mavroidis, C., De Rossi, D., 2008. MRI compatibility of silicone-made contractile dielectric elastomer actuators. *Mechatronics, IEEE/ASME Transactions on* 13, 370–374.
- Chen, D., Cai, S., Suo, Z., Hayward, R.C., 2012. Surface energy as a barrier to creasing of elastomer films: an elastic analogy to classical nucleation. *Physical Review Letters* 109, 038001.

- Gent, A., 2005. Elastic instabilities in rubber. *International Journal of Non-Linear Mechanics* 40, 165–175.
- Gent, A., Cho, I., 1999. Surface instabilities in compressed or bent rubber blocks. *Rubber Chemistry and Technology* 72, 253–262.
- Holmes, D.P., Tavakol, B., Froehlicher, G., Stone, H.A., 2013. Control and manipulation of microfluidic flow via elastic deformations. *Soft Matter* 9, 7049–7053.
- Hong, W., Gao, F., 2013. Crease instability on the surface of a solid, in: *Mechanical Self-Assembly*. Springer, pp. 111–130.
- Hong, W., Zhao, X., Suo, Z., 2009. Formation of creases on the surfaces of elastomers and gels. *Applied Physics Letters* 95, 111901.
- Jin, L., Auguste, A., Hayward, R.C., Suo, Z., 2015. Bifurcation diagrams for the formation of wrinkles or creases in soft bilayers. *Journal of Applied Mechanics* 82, 061008.
- Jin, L., Chen, D., Hayward, R.C., Suo, Z., 2014. Creases on the interface between two soft materials. *Soft Matter* 10, 303–311.
- Jin, L., Suo, Z., 2015. Smoothing creases on surfaces of strain-stiffening materials. *Journal of the Mechanics and Physics of Solids* 74, 68–79.
- Kang, M.K., Huang, R., 2010. Effect of surface tension on swell-induced surface instability of substrate-confined hydrogel layers. *Soft Matter* 6, 5637–5742.
- Kim, S., Laschi, C., Trimmer, B., 2013. Soft robotics: a bioinspired evolution in robotics. *Trends in Biotechnology* 31, 287–294.
- Laschi, C., Cianchetti, M., Mazzolai, B., Margheri, L., Follador, M., Dario, P., 2012. Soft robot arm inspired by the octopus. *Advanced Robotics* 26, 709–727.
- Li, B., Cao, Y.P., Feng, X.Q., Gao, H., 2012. Mechanics of morphological instabilities and surface wrinkling in soft materials: a review. *Soft Matter* 8, 5728–5745.
- Liu, J.L., Feng, X.Q., 2012. On elastocapillarity: a review. *Acta Mechanica Sinica* 28, 928–940.
- Marchese, A.D., Onal, C.D., Rus, D., 2014. Autonomous soft robotic fish capable of escape maneuvers using fluidic elastomer actuators. *Soft Robotics* 1, 75–87.
- Mirfakhrai, T., Madden, J.D.W., Baughman, R.H., 2007. Polymer artificial muscles. *Materials Today* 10, 30–38.
- Park, H.S., Suo, Z., Zhou, J., Klein, P.A., 2012. A dynamic finite element method for inhomogeneous deformation and electromechanical instability of dielectric elastomer transducers. *International Journal of Solids and Structures* 49, 2187–2194.
- Park, H.S., Wang, Q., Zhao, X., Klein, P.A., 2013. Electromechanical instability on dielectric polymer surface: modeling and experiment. *Computer Methods in Applied Mechanics and Engineering* 260, 40–49.
- Plante, J.S., Dubowsky, S., 2006. Large-scale failure modes of dielectric elastomer actuators. *International Journal of Solids and Structures* 43, 7727–7751.
- Roman, B., Bico, J., 2010. Elasto-capillarity: deforming an elastic structure with a liquid droplet. *Journal of Physics: Condensed Matter* 22, 493101.
- Rus, D., Tolley, M.T., 2015. Design, fabrication and control of soft robots. *Nature* 521, 467–475.
- Saksono, P.H., Peric, D., 2006. On finite element modelling of surface tension. variational formulation and applications - part I: quasi-static problems. *Computational Mechanics* 38, 265–281.
- Seifi, S., Park, H.S., 2016. Computational modeling of electro-elasto-capillary phenomena in dielectric elastomers. *International Journal of Solids and Structures* 87, 236–244.
- Shenoy, V., Sharma, A., 2001. Pattern formation in a thin solid film with interactions. *Physical Review Letters* 86, 119.
- Shivapooja, P., Wang, Q., Orihuela, B., Rittschof, D., Lopez, G.P., Zhao, X., 2013. Bioinspired surfaces with dynamic topography for active control of biofouling. *Advanced Materials* 25, 1430–1434.
- Suo, Z., 2010. Theory of dielectric elastomers. *Acta Mechanica Sinica* 23, 549–578.
- Suo, Z., Zhao, X., Greene, W.H., 2008. A nonlinear field theory of deformable dielectrics. *Journal of the Mechanics and Physics of Solids* 56, 467–486.
- Tahoe, 2015. <http://sourceforge.net/projects/tahoe/>.
- Tanaka, T., Sun, S.T., Hirokawa, Y., Katayama, S., Kucera, J., Hirose, Y., Amiya, T., 1987. Mechanical instability of gels at the phase transition. *Nature* 325, 796–798.
- Wang, Q., Tahir, M., Zang, J., Zhao, X., 2012. Dynamic electrostatic lithography: multiscale on-demand patterning on large-area substrates. *Advanced Materials* 24, 1947–1951.
- Wang, Q., Zhang, L., Zhao, X., 2011. Creasing to cratering instability in polymers under ultrahigh electric fields. *Physical Review Letters* 106, 118301.
- Wang, Q., Zhao, X., 2013. Creasing-wrinkling transition in elastomer films under electric fields. *Physical Review E* 88, 042403.
- Wang, Q., Zhao, X., 2014. Phase diagrams of instabilities in compressed film-substrate systems. *Journal of Applied Mechanics* 81, 051004.
- Wang, Q., Zhao, X., 2016. Beyond wrinkles: multimodal surface instabilities for multifunctional patterning. *MRS Bulletin* 41, 115–122.
- Wang, S., Decker, M., Henann, D.L., Chester, S.A., 2016. Modeling of dielectric viscoelastomers with application to electromechanical instabilities. *Journal of the Mechanics and Physics of Solids* 95, 213–229.
- Weiss, F., Cai, S., Hu, Y., Kang, M.K., Huang, R., Suo, Z., 2013. Creases and wrinkles on the surface of a swollen gel. *Journal of Applied Physics* 114, 073507.
- Zhao, X., Suo, Z., 2007. Method to analyze electromechanical instability of dielectric elastomers. *Applied Physics Letters* 91, 061921.
- Zhao, X., Suo, Z., 2009. Electromechanical instability in semicrystalline polymers. *Applied Physics Letters* 95, 031904.
- Zhou, J., Hong, W., Zhao, X., Zhang, Z., Suo, Z., 2008. Propagation of instability in dielectric elastomers. *International Journal of Solids and Structures* 45, 3739–3750.